Methods in Ecology and Evolution

British Ecological Society

Methods in Ecology and Evolution 2011, **2**, 464–476 doi: 10.1111/j.2041-210X.2011.00094.x

Quantifying the sensitivity of camera traps: an adapted distance sampling approach

J. Marcus Rowcliffe[1]*, Chris Carbone[1], Patrick A. Jansen[2,3], Roland Kays[2,4] and Bart Kranstauber[5]

[1]*ZSL Institute of Zoology, Regent's Park, London NW1 4RY, UK;* [2]*Smithsonian Tropical Research Institute, Balboa, Panamá, Panamá;* [3]*Wageningen University, Centre for Ecosystem Studies, Wageningen, the Netherlands;* [4]*New York State Museum, Albany, NY, USA; and* [5]*Department of Migration and Immuno-Ecology, Max Planck Institute for Ornithology, Radolfzell, Germany*

Summary

1. Abundance estimation is a pervasive goal in ecology. The rate of detection by motion-sensitive camera traps can, in principle, provide information on the abundance of many species of terrestrial vertebrates that are otherwise difficult to survey. The random encounter model (REM, Rowcliffe *et al.* 2008) provides a means estimating abundance from camera trap rate but requires camera sensitivity to be quantified.

2. Here, we develop a method to estimate the area effectively monitored by cameras, which is one of the most important codeterminants of detection rate. Our method borrows from distance sampling theory, applying detection function models to data on the position (distance and angle relative to the camera) where the animals are first detected. Testing the reliability of this approach through simulation, we find that bias depends on the effective detection angle assumed but was generally low at less than 5% for realistic angles typical of camera traps.

3. We adapted standard detection functions to allow for the possibility of smaller animals passing beneath the field of view close to the camera, resulting in reduced detection probability within that zone. Using a further simulation to test this approach, we find that detection distance can be estimated with little or no bias if detection probability is certain for at least some distance from the camera.

4. Applying this method to a 1-year camera trapping data set from Barro Colorado Island, Panama, we show that effective detection distance is related strongly positively to species body mass and weakly negatively to species average speed of movement. There was also a strong seasonal effect, with shorter detection distance during the wet season. Effective detection angle is related more weakly to species body mass, and again strongly to season, with a wider angle in the wet season.

5. This method represents an important step towards practical application of the REM, including abundance estimation for relatively small (< 1 kg) species.

Key-words: abundance estimation, animal density, camera detection zone, detection probability, passive infrared motion sensor, Random Encounter Model

Introduction

Camera traps are noninvasive survey devices that record animals as they pass, typically triggered by a passive infrared motion sensor. They are rapidly becoming one of the most important tools in the conservation and ecological studies of terrestrial vertebrates (Rowcliffe & Carbone 2008) and have been used to estimate the abundance of individually marked species (e.g. Karanth *et al.* 2006; Linkie *et al.* 2006; Soisalo & Cavalcanti 2006), for multispecies surveys and species richness inventories (e.g. Silveira, Jacomo, & Diniz-Filho 2003; Tobler *et al.* 2008), and to estimate species' occupancy (e.g. Linkie *et al.* 2007).

In addition, the rate of detection of a species by camera traps (i.e. the raw number of records per unit time) may correlate well with animal density (Carbone *et al.* 2001; Kelly 2008; Rovero & Marshall 2009), suggesting a potential to use trap rate as an index of abundance. However, this approach has been discouraged by some because of the possibility for

*Correspondence author. E-mail: marcus.rowcliffe@ioz.ac.uk
Correspondence site: http://www.respond2articles.com/MEE/

variables other than abundance to influence trap rate (Jennelle, Runge, & MacKenzie 2002; O'Brien & Kinnaird 2008). In particular, Rowcliffe *et al*. (2008) identified that the size of the zone within which animals are detected by cameras' infrared sensors is critical. Recent work has shown that there are a number of factors that might influence this. First, camera trap sensitivity varies between animal species. In particular, smaller-bodied animals are less likely to be sensed (Kelly 2008; Kelly & Holub 2008; Tobler *et al*. 2008). Sensitivity can also vary between camera models (Kelly & Holub 2008) and environmental conditions (no published sources that we are currently aware of). It is also possible that a species' typical behaviour may influence the probability of being photographed. For example, faster-moving species may be less likely to be recorded, although as far as we know, this possibility has not been tested. Behaviour also affects trap rates if cameras are nonrandomly placed, in which case, changes in tendency to frequent the targeted sites, such as trails, because of factors such as human disturbance, might confound any abundance signal in trap rates. However, this bias is avoided by random placement of cameras, and it is in this context that the methods presented here are developed.

All of the aforementioned biases have been cited as reasons why trapping rates are unreliable as indicators of abundance. However, if random camera placement is used, and if it is possible to quantify sensitivity in relation to a range of covariates (e.g. climate, habitat, species and camera characteristics), these sources of bias could be controlled for. In principle, this would allow camera trapping rates to be interpreted as abundance indices with greater confidence. More specifically, the ability to measure camera trap detection zone dimensions for specific survey conditions is a critical step in the application of the random encounter model for estimating animal density (REM, Rowcliffe *et al*. 2008).

In this paper, we develop a method for estimating species- and survey-specific dimensions of the camera trap detection zone. Detection probability is a function of animal position relative to the camera; animals are progressively less likely to be detected as they pass further from the sensor's core field of view, while if cameras are set high relative to the size of the animal, those passing close to the camera may be missed by passing below the field of view. Our method borrows from distance sampling theory (Buckland *et al*. 2001) to account for these complexities, using standard detection functions when there is no reduction in detectability close to the camera, but otherwise using an adapted detection function to account for this process. We use simulated data to validate the performance of this approach. We then apply the model to camera trapping data from the tropical moist forest of Barro Colorado Island, Panama, and show how detection zone dimensions vary with species and environmental variables. We test three hypotheses: (i) larger animals are more likely to trigger cameras than are smaller animals; (ii) animals that move past cameras more slowly are more likely to trigger them than are animals that move faster; and (iii) the sensitivity of camera traps varies seasonally with environmental conditions.

Study site: Barro Colorado Island

Camera traps were deployed on Barro Colorado Island (BCI, 9°9′N, 79°51′W), Republic of Panama, a semi-deciduous moist tropical forest on a former hilltop that was isolated from the mainland by the formation of Gatun Lake to complete the Panama Canal. Roughly half of BCI is covered with old-growth forest and roughly half with late-secondary forest of ca. 90 years old. The climate is seasonal, with a distinct 4-month dry season (January–April) and 2600-mm average annual rainfall (Leigh 1999). BCI has a fairly complete fauna with mammal densities similar to much more remote sites (Wright, Gompper, & De Leon 1994). The only large vertebrate absent today is the white-lipped peccary (*Tayassu pecari*), which was eliminated by poachers in the 1930s (Enders 1939 cited in Wright, Hernandez, & Condit 2007).

Field data

Our field data come from 20 camera traps run for 1 year, from February 2008 to February 2009 (Kays & Slauson 2008). Cameras were placed at randomly selected locations in ten different 1-ha forest plots and moved approximately every 8 days for a total of 6312 trap-nights at 789 locations, recording 17226 animal detections of 25 different species. We used Reconyx RC55 cameras that are triggered with a passive infrared motion sensor and record a digital image, using an infrared flash at night. The 1-ha plots were scattered across the secondary forest part of BCI and varied widely in the abundance of large-seeded tree species (Galvez, Kranstauber, & Kays 2009). Random points within these plots were located by generating coordinates in a computer and finding the corresponding locations in the field with a GPS receiver (Garmin 60CSx). Cameras were mounted on a small tree as close as possible to each randomly selected location. All cameras were mounted around 20 cm off the ground and angled to be parallel to the slope of the ground. The view was maximised by aiming them in the most suitable direction, considered to be one with less vegetation or slope obstructing the view. To ensure random placement with respect to animal movements, no bait or lure were used, nor were attempts made to place cameras on game trails or other features that might have increased capture rates. For every motion trigger event, cameras made 10 low-resolution (1 megapixel) pictures at a frame rate of approximately 1 s^{-1} and could immediately be triggered again without delay, essentially producing a short video clip of animals moving in front of the camera.

To record the position of an animal when it first triggered the camera trap, we examined a subset of the photographs in the field before removing the camera, with the aid of a portable card viewer. We noted the position of the animal that triggered the camera in the first frame relative to nearby landmarks such as trees and rocks and then simply measured the distance and angle to that spot from the camera trap with measuring tape and compass. This yielded 1555 records of animal positions on first detection for 19 species. This subset was chosen systematically, taking measurements for the first three records of each

species at each camera deployment, thus avoiding potential bias in tending to measure records that were more obvious and therefore relatively close to the camera. The analyses below concentrate on nine species for which at least 40 records of position on first detection were available (Table 1). We also measured the speed of animals moving in front of the camera from 2231 video clips. These measurements were also taken in the field before removing a camera, by recording the length of each animal's path through the environment with a measuring tape and dividing this distance by the time between first and last images recording the animal. The geometric mean of these speed measures was then used to define species average speed (J. M. Rowcliffe *et al.* unpublished data). Species average body mass values were taken from BCI animal capture data (R. Kays unpublished data) where possible, otherwise Emmons & Freer (1990) or Reid (1997). Key traits and sample sizes for the nine core species are summarised in Table 1.

Detection sensitivity model

The distribution of photographed animal positions relative to the camera arises from the interaction between their pattern of approach to the camera and the rapidity with which the camera and sensor react to their presence. More specifically, we suppose that observed positions depend on the pattern of variation in instantaneous risk of triggering the sensor across the detection zone, the delay between sensor triggering and picture recording and the distributions of directions and speeds at which animals approach. The motivation for this work is to provide a means of estimating detection zone dimensions for application to REM estimation of abundance (Rowcliffe *et al.* 2008), which defines the detection zone as a sector with radius r and angle θ (Fig. 1a). However, the process just outlined does not readily lend itself to the identification of these parameters. While it should be possible in principle to fit a mechanistic model to animal position data to estimate the parameters of an underlying landscape of instantaneous risk of triggering, it is not clear how effective detection radius and angle values could be derived from such a model.

An alternative way to think about the process is that absolute probability of detection declines with linear and angular distance from the camera, allowing the effective detection zone parameters to be estimated by fitting classic distance sampling detection models (Buckland *et al.* 2001) to distance and angle data. This could make sense if the position data arise from allowing the camera to re-trigger immediately following each record, so that each image represents an independent triggering event. However, this study followed common current practice in setting cameras to take a series of pictures automatically following a trigger, and we therefore only have meaningful information on the position of animals on first capture for each passage. If cameras had a 360 degree field of view, all positions on first capture would likely be clustered around the outer boundary of the detection zone, with none closer in; applying a distance-based approach in this case would clearly give biased results and would likely fail anyway owing to the inappropriate data distribution. However, given that camera detection zones are roughly triangular, with the camera at one corner, animals can approach the camera closely before being detected, and it seems intuitively possible that a distance-based approach could provide reasonably unbiased estimates in practice. In this section, we first examine field data to understand the distribution of angular and radial distances from camera on first record and their relationship to one another; we then develop distance-based algorithms for estimating detection zone dimensions from field data. In the following section, we test the reliability of the approach through simulation.

A critical first step is to determine whether r and θ are independent, or alternatively whether they are correlated, perhaps because the outer edges of the detection zone become weaker at greater distance. Looking at records for agouti, the species with the most records in the BCI data set, we find that there is indeed a negative correlation between distance and angle, resulting from a relative lack of records with both large radius and large angle (Fig. 1b,c). However, this correlation is weak and driven by a small number of extreme records. Removing the top 5% of each measure (open symbols in Fig. 1c) leaves a much weaker and nonsignificant correlation. Given that such extreme records are generally considered lacking in information and are frequently truncated in distance analyses, we conclude that the correlation is not important in practice.

Table 1. Summary of key traits and sample sizes for the nine Panamanian forest mammal species with at least 40 measurements of position on first detection. Sample sizes are given for both records of position on first trigger and speed of movement. For brevity, the abbreviated common names given in brackets are used hereafter

Species	Body mass (kg)	Mean speed (cm s^{-1})	Sample sizes	
			Position	Speed
Mouse unknown species (mouse)	0·1	12·4	43	42
Central American spiny rat *Proechimys semispinosus* (rat)	0·4	14·1	109	135
Red-tailed squirrel *Sciurus granatensis* (squirrel)	0·4	14·6	55	68
Central American agouti *Dasyprocta punctata* (agouti)	3·5	16·0	724	980
White-nosed coati, *Nasua narica* (coati)	4·0	19·3	57	129
Paca *Agouti paca* (paca)	8·0	19·3	137	196
Ocelot *Leopardus pardalis* (ocelot)	11·9	30·3	72	93
Red brocket deer *Mazama temama* (brocket)	22·8	16·4	81	184
Collared peccary *Tayassu tajacu* (peccary)	25·2	16·7	114	272

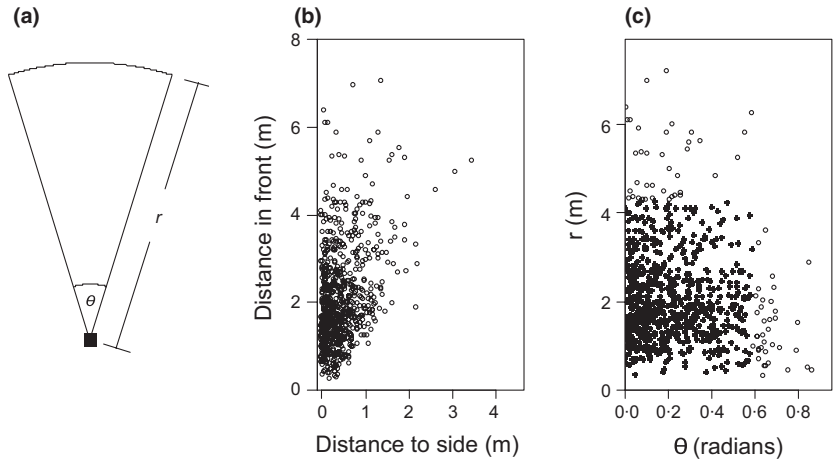

Fig. 1. (a) Diagram of the model used to describe the detection zone (open sector) of a camera trap (filled square). The zone is described by radius r and angle θ. (b) The positions of all agoutis ($n = 724$) on first detection relative to the camera trap (located at co-ordinates 0,0). Note that this plot is a half-sector because we assume that the zone is symmetric. (c) Plot of radial distance from camera (r) against angle (θ) (Pearson correlation coefficient for all records $\rho = -0{\cdot}128$, $P < 0{\cdot}001$; excluding the upper 5th percentile for each measure (open points) $\rho = -0{\cdot}058$, $P = 0{\cdot}13$).

Agoutis most often trigger the camera when they are close to the camera and near to the centre of its angular field of view, with gradual declines in frequency with increasing distance and angle (Fig. 1b). Our detection zone model therefore assumes that sensitivity is greatest close to the camera and near the centre of its field of view and that the probability of the camera reacting to an animal's presence declines monotonically with both distance and angle. Furthermore, following the weak correlation observed between distance and angle, we assume that their effects on detectability are independent of one another. On this basis, declining detectability patterns can readily be modelled using standard distance sampling theory (Buckland *et al.* 2001), using a line transect model for the angle and a point transect model for the distance. We explore the suitability of two possible models for describing detection probability as a function of distance or angle, namely half normal and hazard rate, respectively:

$$a(y) = \exp\left(\frac{-y^2}{2\alpha^2}\right)$$
$$a(y) = 1 - \exp(-(\alpha/y)^{\gamma}) \qquad \text{eqn 1}$$

where $a(y)$ is the detection probability at distance or angle y, α defines the width of the function, and γ in the hazard model defines its shape. We also explored the use of cosine series expansion terms (Buckland *et al.* 2001) to give the functions added flexibility.

A notable characteristic of the distribution of records is that there are fewer than expected very close to the camera trap (note the gap close to the origin in Fig. 1b). This may be either because animals are unwilling or physically unable to pass very close to the tree to which it is attached (most likely to be true for larger animals) or because some animals are missed by passing under the field of view (most likely to be true for smaller animals). In the former case, animals are, in principle, displaced away from the camera rather than missed altogether, so a standard monotonically declining detection model can be fitted to distance data without biasing the result, as long as displaced animals are indeed detected. In the latter case, animals that the model assumes will be recorded are in fact missed, which will bias the result of a standard distance model. For at least some species, we therefore need to adapt the model of variation in detectability with distance to account for this.

To do this, we introduce an additional component to the detection function, describing increasing detectability with distance because of the decreasing probability of passing beneath the field of view. Given that both camera heights within a survey and individual animal sizes within a population will vary, the distance at which animals cease to pass beneath the camera view will also be variable to some degree. Assuming that this variation is approximately normally distributed, we propose that detection probability because of this process $b(r)$ can be characterised by a sigmoid transition from certain nondetection to certain detection with increasing distance and use a logistic model to describe this process:

$$b(r) = \frac{1}{1 + \exp(\delta(\varepsilon - r))} \qquad \text{eqn 2}$$

where δ defines the rate of increase and ε defines its inflection point. The overall probability of detection is then given by the declining detection function $a(y)$ either alone or, if modelling distances for species small enough to pass beneath the field of view, multiplied by the increasing function $b(r)$:

$$g(y) = a(y)\begin{cases} b(r) & y \equiv r \text{ AND species small relative} \\ 1 & \text{otherwise} \end{cases} \qquad \text{eqn 3}$$

Hereafter, we term models with both increasing and decreasing components in the detection function logistic mixture models. Fig. 2 upper row illustrates four scenarios for overall detectability as a function of distance, assuming a hazard rate model for $a(r)$: a) no animals missed close to the camera; b and c)

some animals missed, but a broad or narrow region of certain detectability at intermediate distance; and d) detectability less than certain at all distances.

We fit models to distance and angle data by maximising the likelihood:

$$L(\mathbf{y}) = \prod_{i=1}^{n} f(y_i) \qquad \text{eqn 4}$$

where $\mathbf{y}$ is a data vector (either angles or distances) of length n and $f(y_i)$ is the probability density for a given data point. For angles, probability density is defined by a linear detection process:

$$f(\theta) = \frac{g(\theta)}{\int_0^{\infty} g(\theta)d\theta} \qquad \text{eqn 5}$$

while for distances, probability density is defined by a radial detection process:

$$f(r) = \frac{rg(r)}{\int_0^{\infty} rg(r)dr} \qquad \text{eqn 6}$$

Following standard distance sampling theory, the effective detection angle or distance is estimated by finding the threshold value at which the expected number missed within is equal to the expected number detected beyond. Given threshold angle θ_T, the number missed inside (N_0) is proportional to the area between the detection probability curve and $g(\theta) = 1$ for $\theta < \theta_T$, while the number seen beyond the threshold (N_1) is proportional to the area under the detection probability curve for $\theta > \theta_T$:

$$N_0 \propto \theta_T - \int_0^{\theta_T} g(\theta)d\theta$$
$$N_1 \propto \int_{\theta_T}^{\infty} g(\theta)d\theta \qquad \text{eqn 7}$$

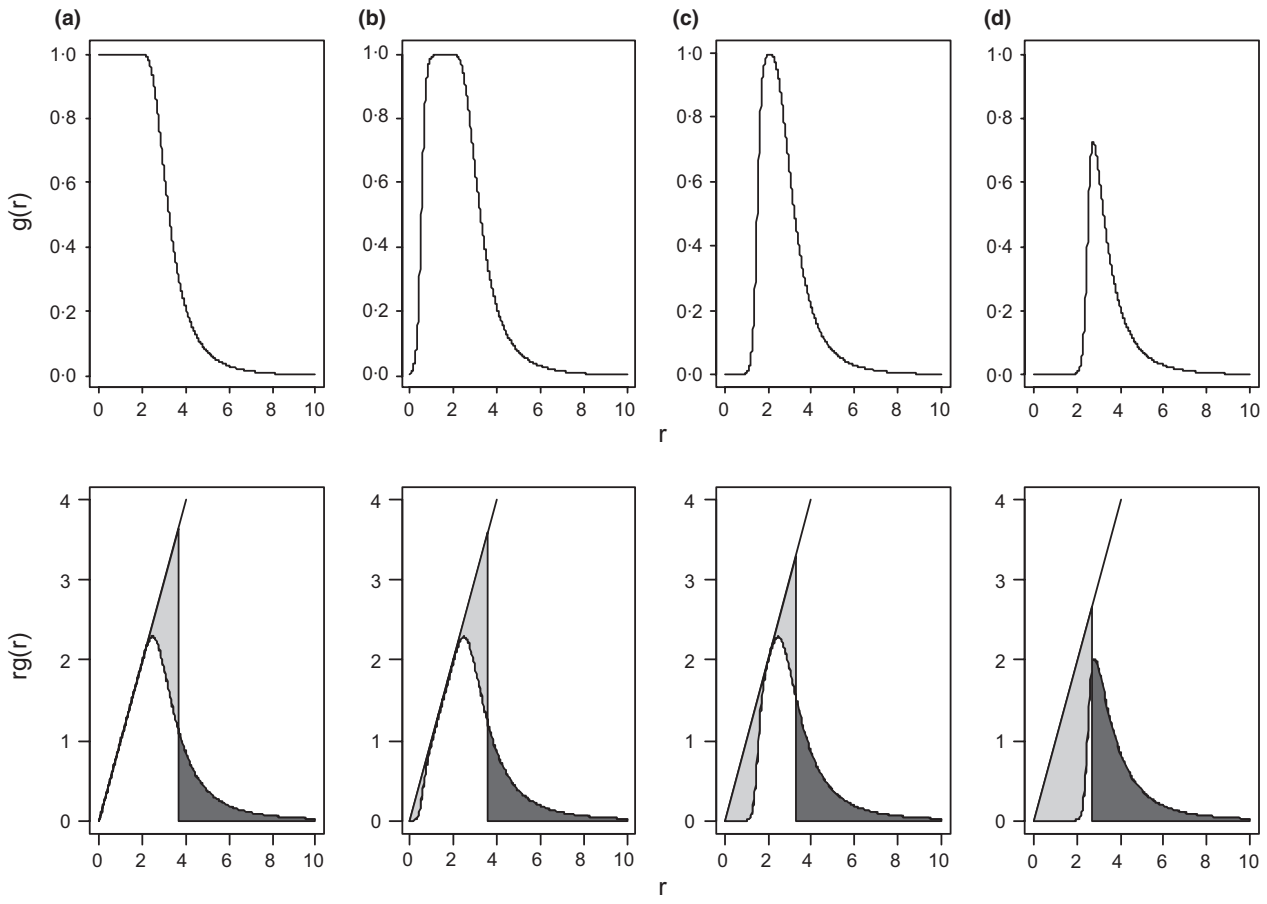

Fig. 2. Upper row: Detection probability as a function of distance, $g(r)$, for four scenarios of detectability close to the camera: (a) certain; (b) uncertain with a broad region of certain detection at intermediate distance; (c) uncertain with a narrow region of certain detection at intermediate distance; (d) uncertain at all distances. Hazard logistic parameters used were $\alpha = 3, \gamma = 5$ and (for b-d) $\delta = 10$; increasing detectability threshold parameters ε were (b) 0·5; (c) 1·5; (d) 2·5. Lower row: The equivalent $rg(r)$ curves for the radial distance model, illustrating the process for calculating the effective detection distance. The diagonal line is defined by $rg(r) = r$; the light-shaded area is proportional to the number of animals present but not detected (N_0); the dark-shaded area is proportional to the number of animals both present and detected (N_1). The vertical dividing line lies at the point where these two areas are equal, giving the effective detection distance: (a) 3·64; (b) 3·6; (c) 3·31; (d) 2·66.

The effective detection angle is estimated by finding the value of θ_T that equalises N_0 and N_1. For distances, the same principle is used, except that a radial detection process is used, so

$$N_0 \propto \frac{r_T^2}{2} - \int_0^{r_T} rg(r)dr$$
$$N_1 \propto \int_{r_T}^{\infty} rg(r)dr \qquad \text{eqn 8}$$

The estimation of effective detection distance is illustrated for four scenarios in Fig. 2 lower row. We estimate the variance of the effective detection distance using the population prediction interval approach, re-sampling model parameter values from the estimated variance/covariance matrix of the fitted detection model.

We also expand the aforementioned models to allow the α and ε parameters in equations 1 and 2 to vary as a function of one or more linear or categorical predictor variables. For example, with k predictor variables:

$$\alpha = \beta_0 + \beta_1 x_1 + \ldots \beta_k x_k \qquad \text{eqn 9)}$$

where β's are parameter coefficients, estimated by maximising the likelihood as described earlier.

Numerical methods implemented in R version 2.11.1 (R Development Core Team 2010) were used for all optimisation and integration problems, using package bbmle for likelihood maximisation (Bolker 2010). The methods developed here can be applied in R using the functions provided in Appendix S1. If logistic mixture models are not required, models can also readily be fitted in program DISTANCE (Thomas *et al.* 2010).

Performance of the detection function approximation

The previous section outlined the motivation for using distance-based detection functions that approximate rather than match the underlying detection process. In this section, we examine the reliability of this approximation by quantifying bias in density estimated using distance-based estimates of effective detection zone dimensions. To do this, we simulate randomised animal paths across a notional camera detection zone, defined by fixed detection radius and angle, outside which risk of capture is effectively zero. Each randomised passage is captured by the camera with probability defined by a two-dimensional landscape of instantaneous risk within the notional detection zone, which also determines the point at which the sensor is triggered for those that are captured. Speed of movement is random, drawn from a log-normal distribution (based on speed measurements reported earlier), and we assume a fixed delay between triggering and registration of the image (a fundamental property of camera traps at present). Full details of the simulation are provided in Appendix S2. This approach generates random observations of position on first record, from which effective detection distance and angle can be estimated. Removing the numerator constant and variables held constant from Eqn. 4 in Rowcliffe *et al.* (2008), relative density can be calculated by:

$$D = \frac{P}{r(2+\theta)}$$

where r and θ are detection zone dimensions as mentioned earlier and P is the number of passages. Using the number of passages detected by the camera and the detection zone dimensions estimated from these records provides an estimate of relative density, while using the total number of passages and fixed dimensions defining the notional detection zone provides a benchmark against which bias can be judged. Bootstrapping this process provides a range of outcomes for a given underlying parameter set, and we report the median percentage bias for a range of widths of camera field of view.

We find that, over most of the range tested, bias is less than 5% (Fig. 3). In particular, subsequent results show estimated effective detection angles in the field of between 15° and 25°, depending on the species (Table 3); within this range, bias is predicted to be between about −4% and 0%, arguably sufficiently low bias to justify the approximation. Substantial positive bias at narrower angles appears to arise because the detection zone approaches a one-dimensional beam, for which a linear rather than radial detection function is more appropriate for estimating effective distance. Radial detection functions tended to fit the data poorly and underestimate effective distance in this case, leading to overestimated relative density.

Performance of the logistic mixture distance model

To assess the ability of the logistic mixture model to estimate effective detection distance accurately, we fitted models to simulated data sets and compared estimated effective detection distances with those defined by the distribution used to generate the data. Based on the observation that hazard models fit

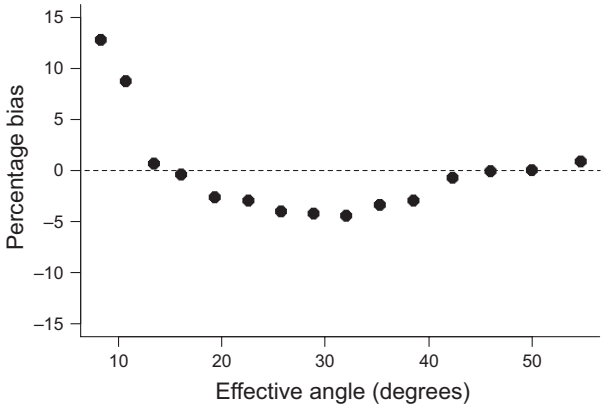

Fig. 3. Percentage bias in relative density, based on detection zone dimensions estimated using a distance-based approximation. Points are the median of 100 bootstrapped estimates on both axes.

distance data from the field well, a hazard logistic model was used both to simulate data sets (by generating random distances drawn from a known distribution) and to fit models to these data. Sample sizes for each data set were either 40 or 200, and three underlying detection functions were explored (those illustrated in Figs 2b–d). This process was repeated 1000 times for each sample size/detection function combination, and the distribution of estimated effective detection distances was compared with the known underlying value.

If the maximum underlying detection probability is less than one, the shape of the probability density function holds no information on the width of the detection plateau or the peak detection probability and fitted models generally fail to give the right answer; there is a tendency for outcomes to converge on detection probability peaks of either one (thus overestimating effective detection distance) or approaching zero (dramatically underestimating effective detection distance). This dichotomy between extreme outcomes is greatest when sample size is low ($\varepsilon = 2{\cdot}5$ and $n = 40$ in Fig. 4), although it is still substantial when there are many observations ($\varepsilon = 2{\cdot}5$ and $n = 200$ in Fig. 4). In the case where peak detection probability is approximately 1, but the peak is a narrow point rather than a broad plateau ($\varepsilon = 1{\cdot}5$ in Figs 2 and 4), the overall outcome is approximately unbiased, but there is still a tendency for models to converge on extremely low effective detection distance estimates. When the underlying detection function has a broad plateau of certain detection probability ($\varepsilon = 0{\cdot}5$ in Figs 2 and 4), outcomes are again approximately unbiased, although there remains a very small chance that the effective detection distance will be massively underestimated if sample size is small.

Detection function forms for tropical forest mammals

Alternative detection functions were explored for the nine species for which we obtained at least 40 records of position on first encounter. Looking first at distance data, hazard rate functions were generally better supported (Table 2). In five species, hazard rate models had the lowest AIC score by at least 3·7 points. The hazard rate model was notably strongly supported in agouti, the species with by far the largest sample ($n = 753$). In three of the four species for which half-normal functions had the lowest AIC, the AIC differences from the equivalent hazard models were relatively small (≤3·7), and chi-squared goodness-of-fit tests suggested no significant lack of fit for hazard models. Only for paca was there strong support for a half-normal model over hazard. However, it seems intuitively sensible that there should be a shoulder of certain detectability up to a certain distance, favouring a hazard model, and we see no reason why the form of the sensitivity should vary between species. We therefore use the hazard rate model in all further analyses of distances.

Logistic mixture models (allowing reduced detectability close to the camera) were best supported in five of the nine species, all with body masses around 4 kg or lower. In contrast, the remaining four species, for which monotonic models were best supported, have body masses of 8 kg or greater. There is thus good evidence that smaller animals were more likely to be missed close to the camera. In none of the species did the addition of cosine expansion terms, allowing greater flexibility in detection function, give a substantially better fit, and we therefore prefer the simple hazard rate function. Detection functions for distance are illustrated in Fig. 5, showing hazard rate model fits, with a logistic modifier where this was statistically justified.

For data on angle at first detection, there was little difference in fit between half-normal and hazard rate models, although the former was generally slightly better supported; we therefore concentrate on the half-normal models for further exploration (Table 3). There was some support for the addition of cosine expansion terms to models for angles. Comparing half-normal models with between 0 and 2 cosine expansion terms, six of the nine species had lowest AICs for models with two terms, notably including agouti (the species with the highest sample size), for which the model with two expansion terms was strongly supported, and the unexpanded half-normal model fitted poorly. For the three species where the unexpanded model was

Table 2. Fits of four alternative detection models to empirical detection distance data for nine mammal species, ordered by body mass. Model fit is judged by AIC and a χ^2 goodness-of-fit test. For each species, the best-fitting model (that with the lowest AIC) is shaded and the corresponding estimate for effective detection distance is provided

	AIC (goodness-of-fit *P*)				
	Half-normal model		Hazard model		
Species	Alone	Logistic mix	Alone	Logistic mix	Effective detection distance (m) (SE)
Mouse	69·0 (0·65)	63·3 (0·92)	68·3 (0·93)	65·6 (0·84)	1·29 (0·27)
Rat	217·1 (0·093)	209·6 (0·702)	207·2 (0·377)	201·5 (0·972)	1·47 (0·13)
Squirrel	137·3 (0·754)	132·8 (0·951)	136·9 (0·862)	133·8 (0·963)	1·88 (0·39)
Agouti	2194·2 (< 0·001)	2164·9 (< 0·001)	2165·9 (0·001)	2144·8 (0·16)	2·54 (0·10)
Coati	177·3 (0·01)	167·7 (0·07)	169·2 (0·17)	158·3 (0·36)	2·11 (0·50)
Paca	431·0 (0·83)	431·2 (0·74)	440·2 (0·02)	441·3 (0·01)	2·55 (0·17)
Ocelot	204·6 (0·71)	206·6 (0·48)	200·5 (0·95)	201·6 (0·92)	2·12 (0·31)
Brocket	297·0 (0·34)	299·6 (0·39)	293·2 (0·57)	296·0 (0·62)	3·64 (0·96)
Peccary	467·0 (0·757)	467·7 (0·566)	470·7 (0·433)	472·3 (0·228)	3·54 (0·44)

Table 3. Fits of three alternative detection models to empirical detection angle data for nine mammal species, ordered by body mass. Model fit is judged by AIC and a χ^2 goodness-of-fit test. For each species, the best-fitting model (that with the lowest AIC) is shaded and the corresponding estimate for effective detection angle is provided

	AIC (goodness-of-fit *P*)			
	Number of cosine expansion terms			
Species	0	1	2	Effective detection angle (degrees) (SE)
Mouse	−52·5 (0·63)	−51·8 (0·7)	−53·1 (0·99)	15·9 (6·4)
Rat	−94·9 (0·14)	−94·0 (0·17)	−100·3 (0·9)	16·5 (3·4)
Squirrel	−50·5 (0·15)	−48·7 (0·17)	−52·4 (0·53)	15·6 (4·89)
Agouti	−753·0 (0·001)	−751·8 (0·002)	−768·2 (0·6)	17·6 (0·9)
Coati	−73·7 (0·44)	−72·3 (0·46)	−72·0 (0·62)	18·9 (1·8)
Paca	−128·7 (0·39)	−127·2 (0·45)	−129·5 (0·72)	17·5 (4·5)
Ocelot	−64·7 (0·17)	−63·2 (0·2)	−65·3 (0·75)	16 (5·4)
Brocket	−79·8 (0·73)	−77·8 (0·73)	−76·5 (0·71)	22·2 (1·8)
Peccary	−90·2 (0·68)	−89·0 (0·87)	−88·6 (0·98)	25·8 (5·8)

best supported, the AIC difference from the two expansion term model was no more than 3·3. As in the case of the distance models, we suggest that the underlying form of the detection function is likely to be consistent across species and therefore adopt the half-normal model with two expansion terms as our standard form for modelling effective detection angles. Model fits are illustrated in Fig. 6, showing a consistent pattern of rapid decline in sensitivity away from the centre of the field of view, but with this rate of decline ameliorating somewhat at intermediate angles.

Correlates of sensitivity for tropical forest mammals

Covariate models show strong support for variation between species and seasons in both effective detection distance and

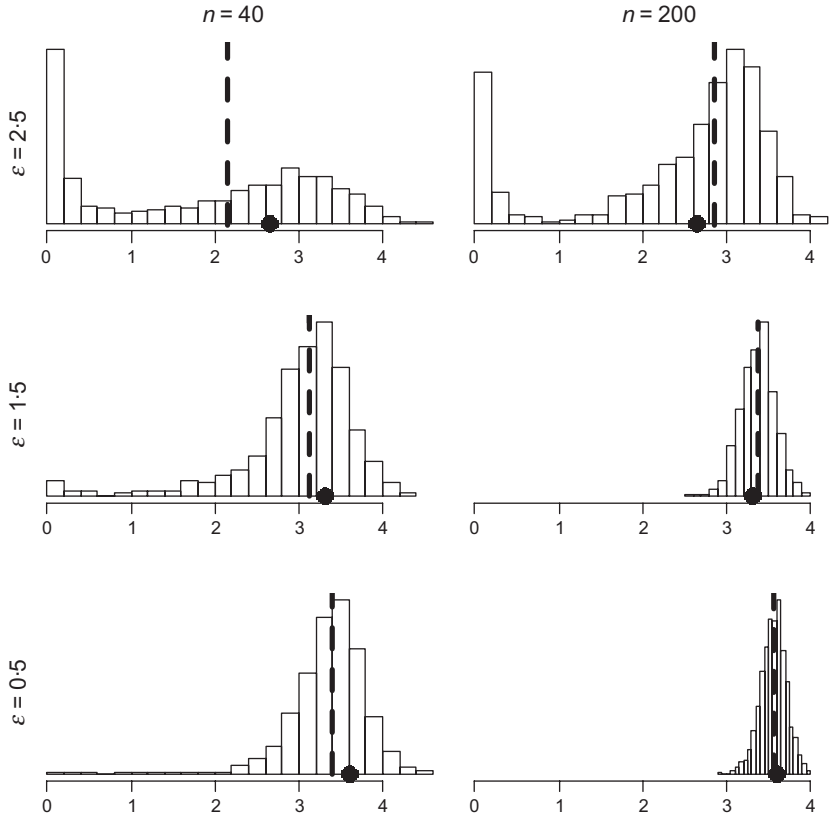

Fig. 4. Frequency distributions (bars) and medians (dashed lines) of estimated effective detection distances from simulated data sets. Filled points indicate the 'true' effective detection distance of the distribution used to generate the data. Sample sizes for each data set were either 40 (left column) or 200 (right column). Three different threshold (ε) parameters were used to generate data sets, defining the likelihood of animals being missed close to the camera (organised by rows, low values indicate a low probability of being missed, see Fig 2b–d for the corresponding detection functions).

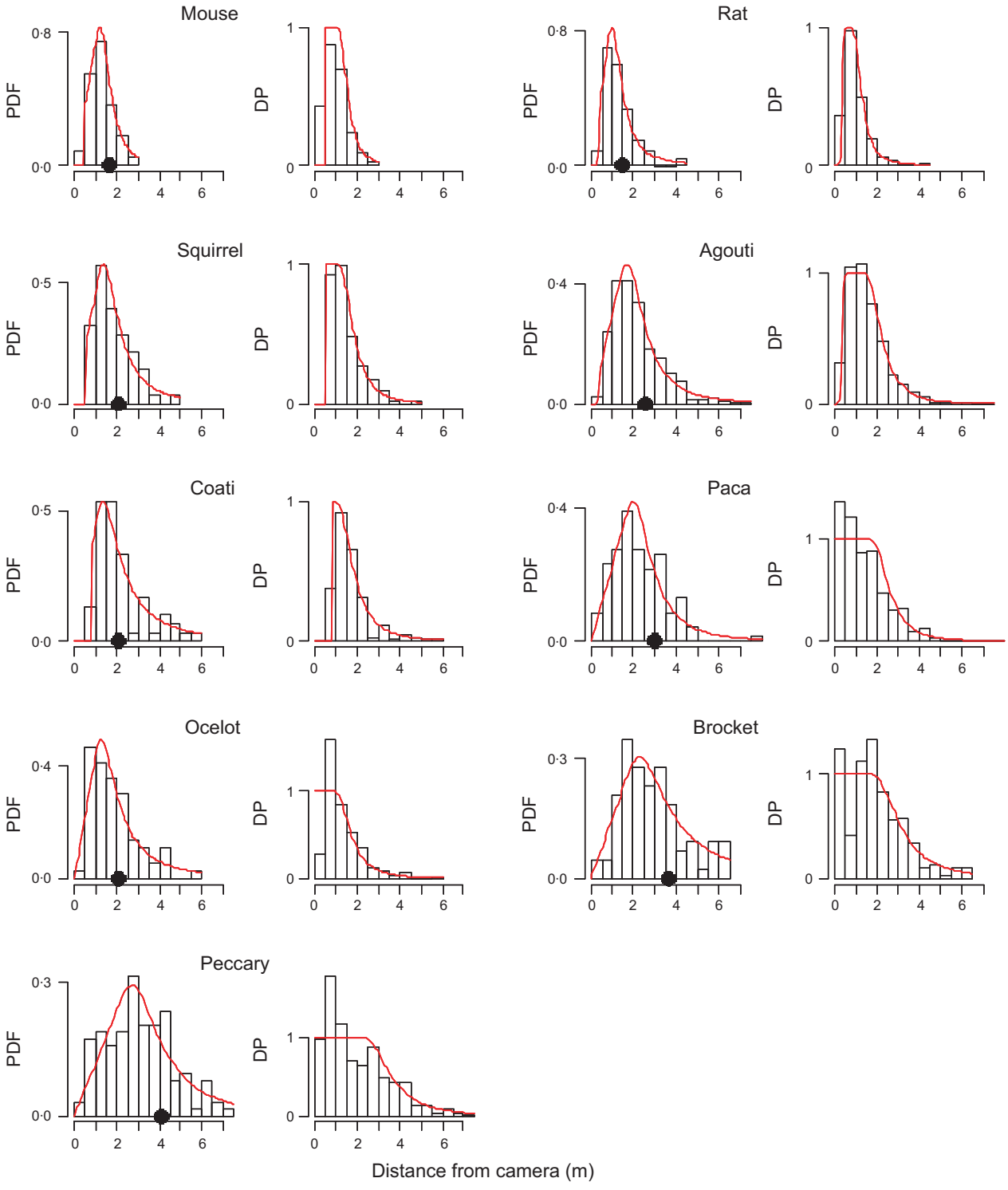

Fig. 5. Probability density functions (PDF) and underlying detection probabilities (DP) for distance from the camera on detection. Bars are density distributions (for PDF) or scaled frequency distributions (for DP) of the data, and curves are defined by the best-fit hazard model, either with or without the logistic element, based on the model AIC (see Table 2). Points on x-axes indicate the estimated effective detection distance. Species are in order of size reading by rows from top left.

angle (Table 4). In the case of angle, variation between species appears to be fully explained by body size (using species mass instead of a categorical species covariate actually improves model support), with no evidence for an effect of species average movement speed. However, for distance, while there was some support for an effect of speed, models including both body mass and speed were much less well supported than those including species identity instead, suggesting that there are some species-specific elements of sensitivity that are not captured by these two traits. There was also some support

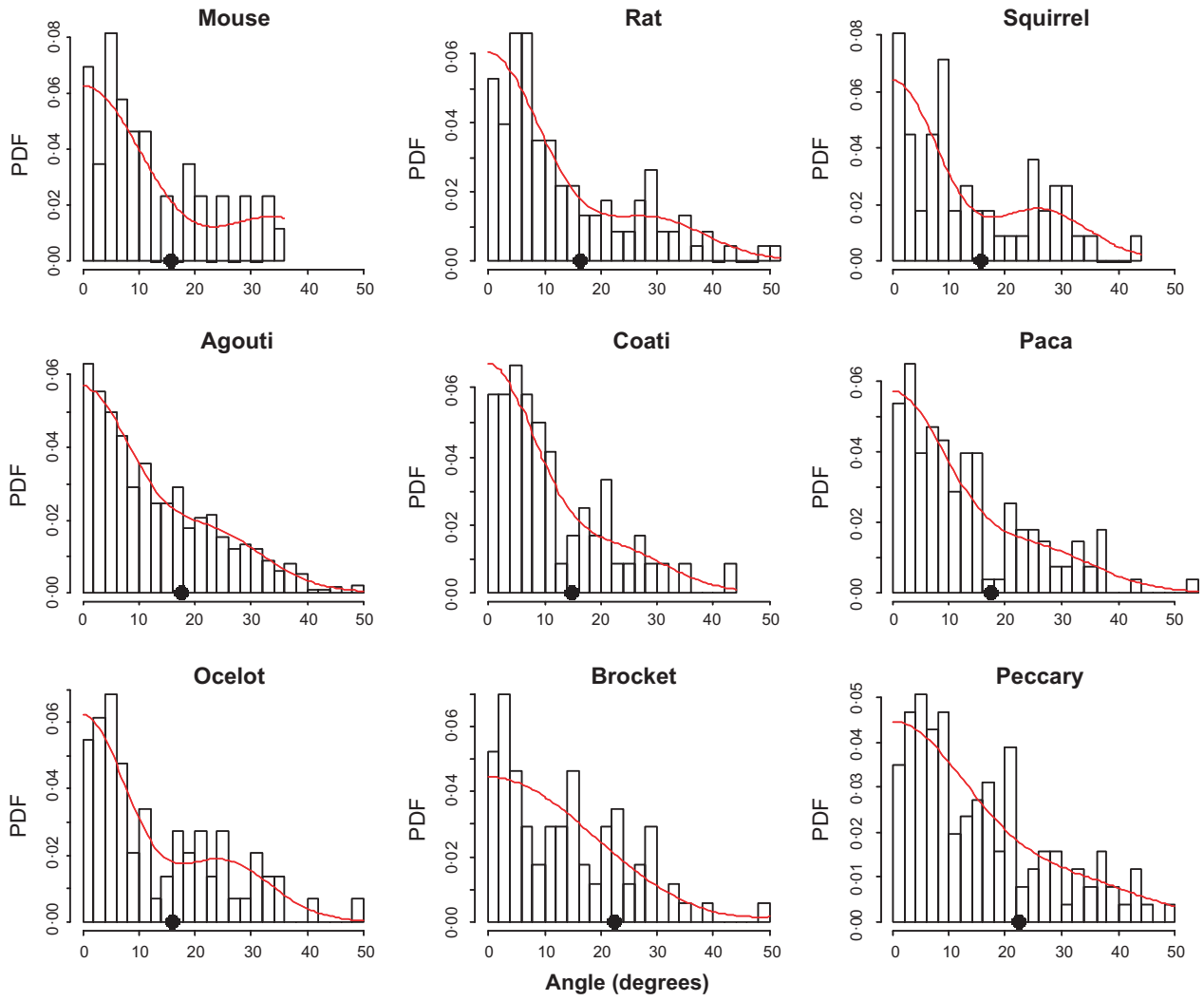

Fig. 6. Probability density functions (PDF) for angle of detection relative to the camera line of sight. Bars are density distributions of the data, and curves are half-normal probability density functions with two cosine expansion terms. Points the on *x*-axis indicate the estimated effective detection angle.

for a linear negative effect of body mass on the threshold detection distance parameter ε, although this effect was relatively weak. This may be because the underlying process is not in fact linear; it is reasonable to expect, and the analyses in Table 2 support this, that animals above a certain size do not have such a detection threshold.

Table 4. Linear model selection summaries for effective detection distance (EDD) and angle (EDA). Both model sets used all observations, including species with fewer than 40 records. The detection function width parameter (α) was modelled as a function of covariates for both distances and angles, while for distances, the threshold distance for detection (ε) was also modelled as a function of mass

	Effective detection distance				Effective detection angle		
	Covariates				Covariates		
Rank	Width (α)	Threshold (ε)	AIC	ΔAIC	Width (α)	AIC	ΔAIC
1	Species, season	Mass	4308·6	0·0	Mass, season	−1582·4	0·0
2	Species, season	.	4311·7	3·1	Mass, speed, season	−1580·4	2·0
3	Species	Mass	4361·2	52·6	Species, season	−1575·0	7·4
4	Mass, speed, season	Mass	4383·6	75·0	Species	−1435·5	146·9
5	Mass, speed	Mass	4438·5	130·0	Mass	−1433·7	148·7
6	Mass	Mass	4443·2	134·6	Mass, speed	−1432·7	149·7
7	Speed	Mass	4576·5	268·0	.	−1426·5	155·9
8	.	Mass	4578·1	269·5	Speed	−1425·2	157·1

Fig. 7 illustrates the trends highlighted by the statistics in Table 4. Effective detection distance increases strongly with the size of the animal (Fig. 7a), with a 2·8-fold difference between the maximum and minimum. The trend for distance with average speed (Fig. 7b) is less clear, as there is relatively little variation in speed and the effect is much weaker than body mass; however, the predicted negative relationship is clear across the four largest species, among which there is more variation in average speed. Effective detection distance becomes shorter as the season becomes wetter, appearing 70% higher during the dry season than during the late wet season, when rainfall is highest (Fig. 7c). Effective detection angle varies less between species (only 50% higher from largest to smallest), and the effect of body mass on angle is weaker than for distance (Fig. 7d); there is no trend in angle with average speed (Fig. 7e). Surprisingly, the effect of season on angle was in the opposite direction to that on distance – effective detection angles were wider in the wet season than in the dry (Fig. 7f). This effect remained consistently clear even when analyses were repeated discarding the 5 or 10% most distant detections, indicating that the result was not an artefact of the weak negative correlation between distance and angle.

Discussion

There are two primary confounding effects that bias trapping rate from randomly placed cameras as an index of abundance (Rowcliffe *et al.* 2008): 1) interspecific variation in activity rate and movement speed and 2) variation in the sensitivity of the camera sensor. We address the former issue in a companion analysis (J. M. Rowcliffe *et al.* unpublished data). In the current paper, we provide methods to account for the latter, making it possible to estimate the dimensions of camera detection zones for very specific species and survey conditions. Because these dimensions equate to those assumed in the random encounter model of abundance (Rowcliffe *et al.* 2008), the results of analyses using these methods can be used directly in REM analyses to provide estimates of animal density.

Our analyses also confirm previous studies (Kelly & Holub 2008; Tobler *et al.* 2008) suggesting that there is substantial variation in camera sensitivity between species and over time, particularly in terms of effective detection distance. Trends in sensitivity parameters were in the hypothesised directions (higher detectability for larger and slower moving species), although we currently have no plausible explanation for why the detection zone becomes shorter but wider as the wet season progresses. The reasons for this pattern, and whether it is a general phenomenon or specific to the cameras used, need further investigation. Variation in sensitivity between species and seasons was substantial, particularly in terms of detection distance, emphasising again the need to estimate detection zone parameters for the specific species and conditions experienced during the survey if sensitivity is to be meaningfully controlled for.

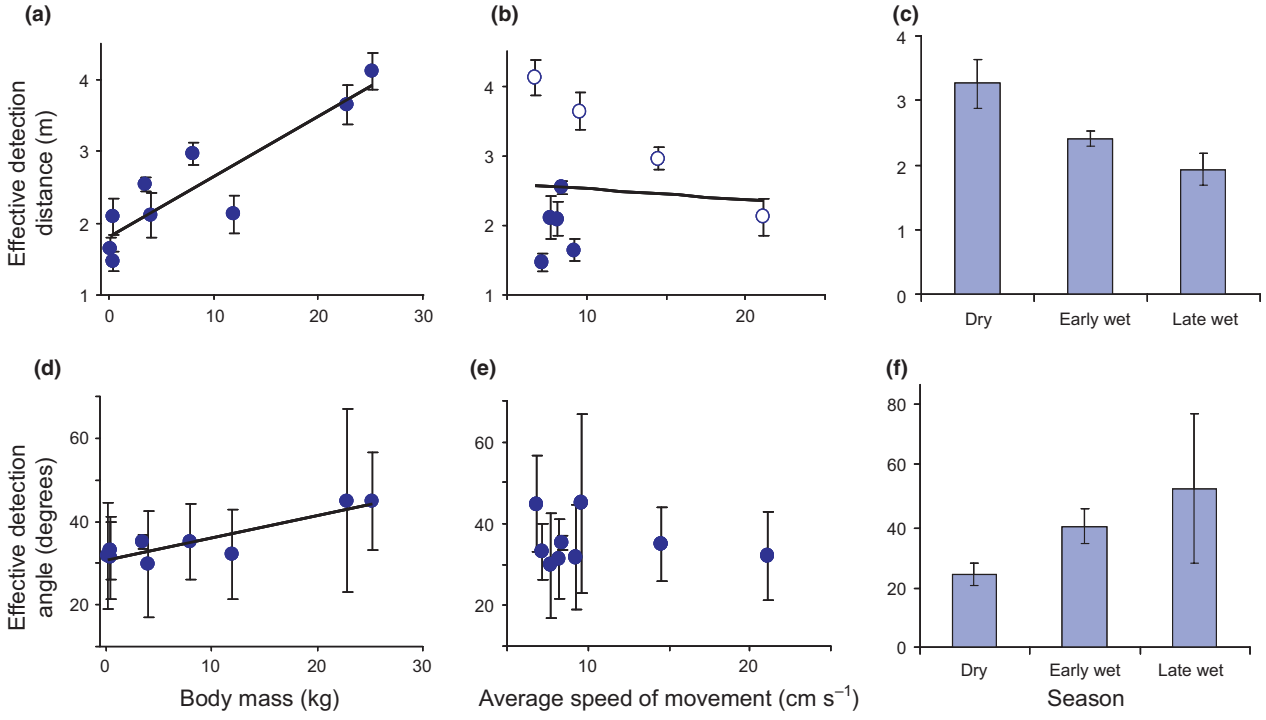

Fig. 7. Effective detection distance (upper row) and angle (lower row) in relation to species body mass (left column), average speed of movement (middle column) and season (right column). Species-specific estimates are derived from the models illustrated in Figs 4 and 5. Season-specific estimates are similarly derived from the hazard logistic model (for distances) or the half-normal model with two cosine expansion terms (for angles), applied to data pooled across species and split by season. Error bars are standard errors. Trend lines are linear regressions fitted to the points to highlight the direction of trends. In b, the four largest species are highlighted with open symbols.

The ability to quantify sensitivity also opens the possibility of using camera traps to estimate the abundance of much smaller species than previously thought. Because of an assumption (usually implicit) that detectability is too uncertain for smaller species, few previous studies have considered using camera traps to obtain data on them (but see Oliveira-Santos, Tortato, & Graipel 2008; De Bondi *et al*. 2010). However, in this case, we were able to obtain useable data on species as small as 100 g mice and make credible estimates of detection zone dimensions, enabling the uncertainty in detectability to be quantified and controlled for.

An important caveat regarding the use of this method for very small species is that the logistic mixture model of variation in detectability with distance is unreliable if detectability is nowhere certain. This could be avoided by setting the cameras as low as possible in cases where smaller species are to be targeted and angling the camera slightly downwards, thus minimising or eliminating the possibility of animals passing beneath the field of view. This is different from the current practice in which cameras are usually put at around 30 cm or even higher (e.g. O'Brien, Kinnaird, & Wibisono 2003; Srbek-Araujo & Chiarello 2005). Alternatively, where data on multiple species are obtained, as in this case, a multispecies covariate model with body mass covariate might be used to extrapolate the detection function shape for smaller species to give an unbiased estimate of effective detection distance, even where detection probability never approaches 1 in any part of the detection zone. Further work is needed to evaluate the reliability of this possible approach.

It should also be noted that detection probability might be less than 1 throughout the detection zone if sensors are very slow or unreliable in their responses. In this case, the methods developed here would give biased estimates of effective detection zone dimensions. The cameras used in this study appeared to have reliably rapid responses (c. 0·1 s), and we therefore believe that the assumption of certain detectability at the heart of the detection zone was reasonable; however, this may not be the case for all camera models. Researchers should satisfy themselves that their cameras are responding sufficiently reliably to animals passing close by before using the logistic mixture model. Controlled trials of camera responses to captive animals of a similar size to those targeted in the field would be a possible way to achieve this.

One further constraint is the effort required to gather the position data required. This adds significant additional time costs in the field, and we are therefore developing tools to extract the necessary information by automated analysis of images once downloaded (see Kays & Slauson 2008 for a preliminary description of this approach).

Acknowledgements

We thank Nadia Sitas, Anthony Turner, Daniel Rasmussen and Lennart Suselbeek for assistance in the field and the Smithsonian Tropical Research Institute, especially Oris Acevedo, for general logistical support. Required permits for the work described in this paper were obtained from the Autoridad Nacional del Ambiente, Panama, and the Smithsonian Tropical Research Institute. We are indebted to three referees for their insightful and supportive comments, in particular Steve Buckland. The work was funded by NSF (DEB 0717071) and the British Ecological Society. PAJ was funded by the Netherlands Foundation of Scientific Research (NWO-ALW 863-07-008).

References

Bolker, B.M. (2010) Tools for general maximum likelihood estimation. http://CRAN.R-project.org/package = bbmle.

Buckland, S.T., Anderson, D.R., Burnham, K.P., Laake, J.L., Borchers, D.L. & Thomas, L. (2001) *Introduction to Distance Sampling: Estimating Abundance of Biological Populations*. Oxford University Press, Oxford.

Carbone, C., Christie, S., Coulson, T., Franklin, N., Ginsberg, J.R., Griffiths, M., Holden, J., Kawanishi, K., Kinnaird, M.F., Laidlaw, R., Lynam, A., Macdonald, D.W., Martyr, D., McDougal, C., Nath, L., Obrien, T., Seidensticker, J., Smith, D.J.L., Sunquist, M., Tilson, R. & Wan Shahruddin, W.N. (2001) The use of photographic rates to estimate densities of tigers and other cryptic mammals. *Animal Conservation*, **4**, 75–79.

De Bondi, N., White, J.G., Stevens, M. & Cooke, R. (2010) A comparison of the effectiveness of camera trapping and live trapping for sampling terrestrial small-mammal communities. *Wildlife Research*, **37**, 456–465.

Emmons, L.H. & Freer, E. (1990) *Neotropical Rainforest Mammals: A Field Guide*. University of Chicago Press, Chicago.

Galvez, D., Kranstauber, B. & Kays, R.W. (2009) Scatter hoarding by the Central American agouti: a test of optimal cache spacing theory. *Animal Behaviour*, **78**, 1327–1333.

Jennelle, C.S., Runge, M.C. & MacKenzie, D.I. (2002) The use of photographic rates to estimate densities of tigers and other cryptic mammals: a comment on misleading conclusions. *Animal Conservation*, **5**, 119–120.

Karanth, K.U., Nichols, J.D., Kumar, N.S. & Hines, J.E. (2006) Assessing tiger population dynamics using photographic capture-recapture sampling. *Ecology*, **87**, 2925–2937.

Kays, R.W. & Slauson, K.M. (2008) Remote cameras. *In Noninvasive Survey Methods for Carnivores* (eds R.A. Long, P. MacKay, W.J. Zielinski & C.J. Ray), pp. 110–140. Island Press, Washington D.C.

Kelly, M.J. (2008) Design, evaluate, refine: camera trap studies for elusive species. *Animal Conservation*, **11**, 182–184.

Kelly, M.J. & Holub, E.L. (2008) Camera trapping carnivores: trap success among camera types and across species, and habitat selection by species on salt pond mountain, Giles Co., VA. *Northwestern Naturalist*, **15**, 249–262.

Leigh, E.G. (1999) *Tropical Forest Ecology : A View From Barro Colorado Island*. Oxford University Press, New York.

Linkie, M., Chapron, G., Martyr, D.J., Holden, J. & Leader-Williams, N. (2006) Assessing the viability of tiger subpopulations in a fragmented landscape. *Journal of Applied Ecology*, **43**, 576–586.

Linkie, M., Dinata, Y., Nugroho, A. & Achmad Haidir, L. (2007) Estimating occupancy of a data deficient mammalian species living in tropical rainforests: Sun bears in the Kerinci Seblat region, Sumatra. *Biological Conservation*, **137**, 20–27.

O'Brien, T.G. & Kinnaird, M.F. (2008) A picture is worth a thousand words: the application of camera trapping to the study of birds. *Bird Conservation International*, **18**, S144–S162.

O'Brien, T.G., Kinnaird, M.F. & Wibisono, H.T. (2003) Crouching tigers, hidden prey: Sumatran tiger and prey populations in a tropical forest landscape. *Animal Conservation*, **6**, 131–139.

Oliveira-Santos, L.G.R., Tortato, M.A. & Graipel, M.E. (2008) Activity pattern of Atlantic Forest small arboreal mammals as revealed by camera traps. *Journal of Tropical Ecology*, **24**, 563–567.

R Development Core Team (2010) R: A language and environment for statistical computing. R Foundation for Statistical Computing, Vienna, Austria, http://www.R-project.org.

Reid, F. (1997) *A Field Guide to the Mammals of Central America and Southeast Mexico*. Oxford University Press, Oxford.

Rovero, F. & Marshall, A.R. (2009) Camera trapping photographic rate as an index of density in forest ungulates. *Journal of Applied Ecology*, **46**, 1011–1017.

Rowcliffe, J.M. & Carbone, C. (2008) Surveys using camera traps: are we looking to a brighter future? *Animal Conservation*, **11**, 185–186.

Rowcliffe, J.M., Field, J., Turvey, S.T. & Carbone, C. (2008) Estimating animal density using camera traps without the need for individual recognition. *Journal of Applied Ecology*, **45**, 1228–1236.

Silveira, L., Jacomo, A.T.A. & Diniz-Filho, J.A.F. (2003) Camera trap, line transect census and track surveys: a comparative evaluation. *Biological Conservation*, **114**, 351–355.

Soisalo, M.K. & Cavalcanti, S.M.C. (2006) Estimating the density of a jaguar population in the Brazilian Pantanal using camera-traps and capture–recapture sampling in combination with GPS radio-telemetry. *Biological Conservation*, **129**, 487–496.

Srbek-Araujo, A.C. & Chiarello, A.G. (2005) Is camera trapping an efficient method for surveying mammals in Neotropical forests? A case study in south-eastern Brazil *Journal of Tropical Ecology*, **21**, 121–125.

Thomas, L., Buckland, S.T., Rexstad, E.A., Laake, J.L., Strindberg, S., Hedley, S.L., Bishop, J.R.B., Marques, T.A. & Burnham, K.P. (2010) Distance software: design and analysis of distance sampling surveys for estimating population size. *Journal of Applied Ecology*, **47**, 5–14.

Tobler, M.W., Carrillo-Percastegui, S.E., Leite Pitman, R., Mares, R. & Powell, G. (2008) An evaluation of camera traps for inventorying large- and medium-sized terrestrial rainforest mammals. *Animal Conservation*, **11**, 169–178.

Wright, S. J., Gompper, M.E. & De Leon, B. (1994) Are large predators keystone species in neotropical forests? The evidence from Barro Colorado Island. *Oikos*, **71**, 279–294.

Wright, S.J., Hernandez, A. & Condit, R. (2007) The bushmeat harvest alters seedling banks by favoring lianas, large seeds, and seeds dispersed by bats, birds, and wind. *Biotropica*, **39**, 363–371.

Received 10 September 2010; accepted 24 January 2011
Handling Editor: David Orme

Supporting Information

Additional Supporting Information may be found in the online version of this article.

Appendix S1. R functions for fitting standard and linear covariate detection models to position on first capture by camera traps.

Appendix S2. Method for generating simulated camera trap data on position of first trigger.

As a service to our authors and readers, this journal provides supporting information supplied by the authors. Such materials may be re-organised for online delivery, but are not copy-edited or typeset. Technical support issues arising from supporting information (other than missing files) should be addressed to the authors.